



Plasmonic enhanced multifunctional composite photoanode for highly efficient dye-sensitized solar cells

M. A. K. L. Dissanayake¹ · S. Senthuran^{1,2,3} · G. K. R. Senadeera^{1,4}

Received: 18 May 2024 / Revised: 17 January 2025 / Accepted: 10 February 2025
© The Author(s), under exclusive licence to Springer-Verlag GmbH Germany, part of Springer Nature 2025

Abstract

Dye-sensitized solar cells (DSSCs) were fabricated using different photoanode compositions of P25 TiO₂ and hierarchically structured TiO₂ microspheres and optimized their performance. DSSCs fabricated with 10% TiO₂ microspheres in the composite photoanode exhibited the highest efficiency of 7.17%, while the devices with pristine P25 TiO₂ photoanode showed an efficiency of 6.34% under the same illumination conditions of 100 mW cm⁻². Device performance was further optimized by using the plasmonic effect of Ag nanoparticles (AgNPs) with different particle sizes. SEM imaging revealed that the average diameter of the TiO₂ microspheres was about 700 nm and consisted of aggregates of smaller TiO₂ nanoparticles of diameters 5–15 nm. This unique morphology appears to enhance the light absorption by scattering effect as well as by increasing the specific surface area of the TiO₂ photoanode for improved dye adsorption. The average particle size of the Ag nanoparticles confirmed by the Transmittance Electron Microscopy (TEM) measurements was found to be 20 nm (red colour) and 80 nm (blue colour). Optimized DSSCs made with 10 wt% of AgNPs (in TiO₂) with red colour and blue colour showed efficiencies of 7.88% and 8.15% respectively under the same illumination conditions. An impressive ~29% increase in the overall device efficiency due to the combined effect of hierarchically TiO₂ microspheres as well as the plasmonic Ag NPs of blue colour (cluster size 80 nm) in the photoanodes, whereas the overall efficiency enhancement with red-coloured AgNPs of size ~20 nm was ~24%.

Keywords Dye-sensitized solar cells · Hierarchical TiO₂ micro spheres · Composite photoanode · Silver nanoparticles · Plasmonic solar cells

Introduction

Since the breakthrough seminal work reported by O'Regan and Gratzel in 1991 [1], dye-sensitized solar cells (DSSCs) have attracted a great deal of interest among the scientific

community and intensively researched by many research groups around the world as an alternative photovoltaic technology to the conventional silicon-based technology due to the low-cost, simple, and environmentally friendly fabrication process combined with promising power conversion efficiencies [2–5]. A DSSC typically consists of a mesoporous nanocrystalline, wide band gap semiconductor metal oxide layer deposited on a transparent conducting oxide substrate (TCO) usually on a glass plate with a thin film of fluorine-doped SnO₂ layer, dye sensitizer, redox electrolyte, and a counter electrode fabricated all together in a sandwich structure. The light is absorbed by the dye sensitizer, and the excited dye molecules transfer the electrons into the conduction band of the metal oxide semiconductor. The transferred electrons are then percolated through the metal oxide semiconductor layer to an external circuit through which they are transported to the catalytic counter electrode in the other side of the device. The redox electrolyte is regenerated at the counter electrode with these

Highlights Dye-sensitized solar cells with P25 TiO₂ photoanode showed an efficiency of 6.34%.

Photoanode incorporating 10% TiO₂ microspheres showed the highest cell efficiency of 7.17%.

The incorporation of 10 wt% of blue AgNPs further enhanced the efficiency to 8.15%.

Twenty-nine percent increase in efficiency was achieved due to TiO₂ microspheres and blue Ag NPs.

Statement of novelty To the best of our knowledge, this is the first report of efficiency enhancement in dye sensitized solar cells caused by the 'combined effect' of TiO₂ mesospheres acting as a scattering layer along with the plasmonic effect by silver nanoparticles.

Extended author information available on the last page of the article

electrons, and the dye is regenerated by electrons donated from the species in the redox electrolyte (I^-) [3].

A significant amount of research has been directed towards improving the performance of DSSCs by optimizing the light-harvesting capability of the photoanodes such as the synthesis of broader absorption band sensitizers [4–9] developing quasi-solid/solid electrolytes [10, 11], and designing Pt-free counter electrodes [12, 13]. However, the photoanode plays a crucial role in the overall power conversion efficiency of the solar cell because both dye adsorption and electron transport take place in the photoanode. Thus, optimizing the architecture of the photoanode for efficient light harvesting is one of the key strategies to enhance the efficiencies of DSSCs. A photoanode with a high specific surface area, fast electron transport pathways, and a pronounced light scattering scheme is desirable for achieving higher efficiencies [3]. The typical mesoporous photoanode made of 15–20 nm diameter TiO_2 nanoparticles provides a large internal surface area for the attachment of a large number of dye molecules on the photoanode [14].

Since the light absorption of the dye molecules are limited to a certain specific wavelength regions and the wide band gap semiconductors are not capable of capturing the photons effectively, these dye-sensitized photoanodes are not able to capture the photons in the entire solar spectrum, especially in the longer wavelength region [15, 16]. To overcome this problem, a scattering layer containing a larger diameter (~400 nm) TiO_2 particles is sometimes placed on top of the transparent active layer to scatter back the light incident on the photoanode [17–19]. Notable morphologies of TiO_2 that are widely used for such scattering layers are nano-wires [20], nano-rods [21], nano-tubes [22], nano-fibers [23], nano-sheets [24], nano-spindles [9], and solid and hollow microspheres [25–27]. However, these scattering layers cannot enhance the dye adsorption adequately because of the limited specific surface area due to larger size particles in the scattering layer. Such solid microspheres also increase the thickness of the photoanode due to which the interfacial resistance of the photoanode increases thereby limiting the open circuit photovoltage.

Because of the above-mentioned issues, large internal surface area, superior light-scattering effect, and fast electron transport are believed to be indispensable for a photoanode to achieve higher efficiencies in a DSSC. However, these three factors are often incompatible with one another. Therefore, one of the most appropriate approaches to overcome this problem is to produce a multifunctional photoanode that can offer a large surface area, good light-scattering and absorption ability, and fast electron transport properties simultaneously. This could be achieved by fabricating a composite photoanode structure with a mixture of small and large particles in an optimal proportion. The optical path length of incident light in the composite photoanode can

be increased significantly with minimal thickness. Among these, composite photoanodes of DSSCs made of nanowire-nanoparticle [28, 29], nanotube-nanoparticle [30], nanofibre-nanoparticle [31], nanorod-nanoparticle [32], and spherical TiO_2 nanorod aggregate-nanoparticle [33] have already been demonstrated with higher efficiencies than DSSCs made of conventional photoanodes made of ~20 nm TiO_2 particles. By considering these factors, in this study, structurally modified photo anodes were further modified using the plasmonic effect associated with the Ag nanoparticles using a simple drop-casting method [27, 33–35] in order to further enhance the device performance. To the best of our knowledge, this is the first report on plasmonic enhanced multifunctional composite photoanode-based dye-sensitized solar cells. An impressive ~29% increase in the overall device efficiency is achieved due to the combined effect of hierarchically TiO_2 microspheres as well as the plasmonic Ag NPs of blue colour (80 nm) in the photoanodes.

Experimental

Materials

Fluorine-doped tin oxide (FTO)-coated conducting glasses ($8 \Omega \text{ cm}^{-2}$, Solaronix), titanium (IV) isopropoxide (97% Fluka), titanium dioxide P-90 powder (Evonik), titanium dioxide powder P-25 (Degussa), poly ethylene glycol (PEG-1000, 99.8%, Sigma-Aldrich), Triton X-100 (Sigma-Aldrich), ethanol absolute (anhydrous, > 99.8%, VWR Chemicals), glacial acetic acid (99%, Fisher), ethylene carbonate (EC, Fluka), tetrapropyl ammonium iodide (Pr_4NI , Sigma-Aldrich), iodine chips (I_2 , Fluka), ruthenium dye (N719, Solaronix), silver nitrate ($AgNO_3$, Sigma-Aldrich), N,N-dimethyl formamide (DMF, 99.5%, BDH Chemicals), and polyvinyl pyrrolidone (PVP, Mw = 44,000, BDH Chemicals) were used as received.

Synthesis of TiO_2 microspheres (TiO_2 -MS)

Hierarchically structured mesoporous TiO_2 microspheres were synthesized through controlled hydrothermal treatment of titanium (IV) isopropoxide (TTIP) in ethanol-glacial acetic acid mixture as reported elsewhere [25]. Typically, 1.0 ml TTIP was added drop-wise into a mixed solvent of acetic acid (10 ml)–ethanol (50 ml) under vigorous stirring (1 h) at room temperature. The clear solution obtained was transferred into 100 ml Teflon-lined stainless steel autoclave, and hydrothermal treatment was performed at 180 °C for 9 h. Then, the autoclave was allowed to cool down to room temperature. The resulting white precipitate was collected by centrifuging and subsequently washed with ethanol and distilled water several times and then dried overnight at 90

°C. Finally, the powder sample was calcined at 400 °C for 3 h in a furnace to obtain the TiO₂ microspheres.

Synthesis of silver nanoparticles (Ag NPs)

Silver nanoparticles (Ag NPs) with different sizes were synthesized by chemical reduction method using DMF route as reported elsewhere [34]. In brief, firstly, 0.85 g PVP was dissolved in 20 ml DMF solvent. Then, 0.25 mg AgNO₃ was added into the DMF–PVP mixture at room temperature. After the solution turned to yellow color, the mixture was heated at 90 °C under continuous stirring. During the heating process, the colour of the mixture changed to red, and then to blue and green with increase in heating time. The appropriate amount of the mixture with each colour was transferred to the test tube. After the mixture was allowed to cool down to room temperature, it was centrifuged at 3000 rpm using acetone as a precipitating agent. Finally, an appropriate amount of the precipitate was dispersed in ethanol to get 0.10%(W/V) AgNPs. The concentrated AgNP colloidal solution was sonicated for 30 min before applying to the DSSCs to ensure the uniform dispersion of AgNPs in ethanol.

Preparation of composite photoanodes

To study the effect of the hierarchical TiO₂ microspheres on the performance of DSSCs, four composite photoanodes consisting of P25 TiO₂ nanoparticles and hierarchical TiO₂ microspheres (MS) (labelled as P25 only, 5% MS, 10% MS and 15% MS) were prepared with hierarchical TiO₂ microsphere concentrations of 0, 5, 10, and 15 wt%, respectively. The detailed procedure for the photoanode preparation is described elsewhere [35].

Preparation of the liquid electrolyte

The iodide/triiodide-based liquid electrolyte used for this work was prepared by dissolving 0.738 g tetrapropylammonium iodide (Pr₄NI), 0.06 g iodine (I₂) and 3.6 ml of molten ethylene carbonate (EC) in 1 ml acetonitrile. The final mixture was magnetically stirred for 24 h at room temperature for 30 min.

Characterization of photoanode and solar cells

The surface morphologies of photoanodes were characterized by scanning electron microscopy (SEM) using Zeiss EVO LS15 electron microscope. The wide-angle X-ray spectroscopy (WAXS) was performed using a Rigaku X-ray diffractometer with CuK α radiation ($\lambda = 1.5406 \text{ \AA}$). The diffuse reflection spectra were obtained in the wavelength range from 240 to 800 nm using a UV–Vis spectrophotometer

(Shimadzu 2450) with an integrating sphere attachment. The current density–voltage (*J*–*V*) measurements of solar cells were performed with a Keithley 2400 source meter (Keithley Instruments, USA) with solar simulator (Oriel) under 100 mWcm⁻² (one sun) illumination with AM 1.5 spectral filter. The solar simulator was calibrated with a silicon photodiode (Hamamatsu Photonics, Japan). The active area of a solar cell was kept as 0.25 cm². The interfacial charge transfer resistances and electron lifetime were estimated by electrochemical impedance spectroscopy (EIS) performed under 100 mW cm⁻² illumination using a Metrohm Autolab PGSTAT128N in potentiostat mode with a FRA 32 M frequency response analyzer covering the wide frequency range from 0.01 Hz to 1 MHz. The external quantum efficiency (EQE) measurements were done on Bentham PVE300 IPCE unit with a xenon arc lamp.

Results and discussion

SEM analysis of TiO₂ microspheres (TiO₂-MS)

The morphology and nanostructure of the synthesized mesoporous TiO₂ microspheres were first examined by scanning electron microscopy (SEM). As seen in Fig. 1 the TiO₂ microspheres consist of well-defined spherical sub-micron size structures composed of aggregates of TiO₂ nanoparticles. The average diameter of the microspheres is about 700 nm. The diameter of the microspheres can be controlled by controlling the volume ratio of the solvents used in the solution while keeping other hydrothermal conditions unchanged. Figure 1b shows a high-resolution SEM image of a single TiO₂ microsphere. A closer inspection of Fig. 1b reveals that the size of the constituent TiO₂ nanoparticles ranges between 5 and 15 nm, which is favourable for dye adsorption because of the very high specific surface area compared to a normal TiO₂ P25 photoanode with particle sizes around 25 nm.

SEM analysis of MS/P25 composite photoanode

Figure 2 illustrates the schematic diagrams of four different types of photoanodes with microspheres as light scatterers. While Fig. 2A shows the structure of a photoanode fabricated with larger microspheres for light scattering mixed with smaller nanoparticles, Fig. 2B shows the structure of a photoanode fabricated with a layer of microspheres deposited on top of a conventional-type transparent TiO₂ nanoparticle layer to act as a scattering layer for backscattering. Figure 2C shows photoanodes fabricated with only hierarchically structured TiO₂ microspheres for achieving both high surface area as well as improved light scattering. Figure 2D shows a photoanode consisting of hierarchically structured

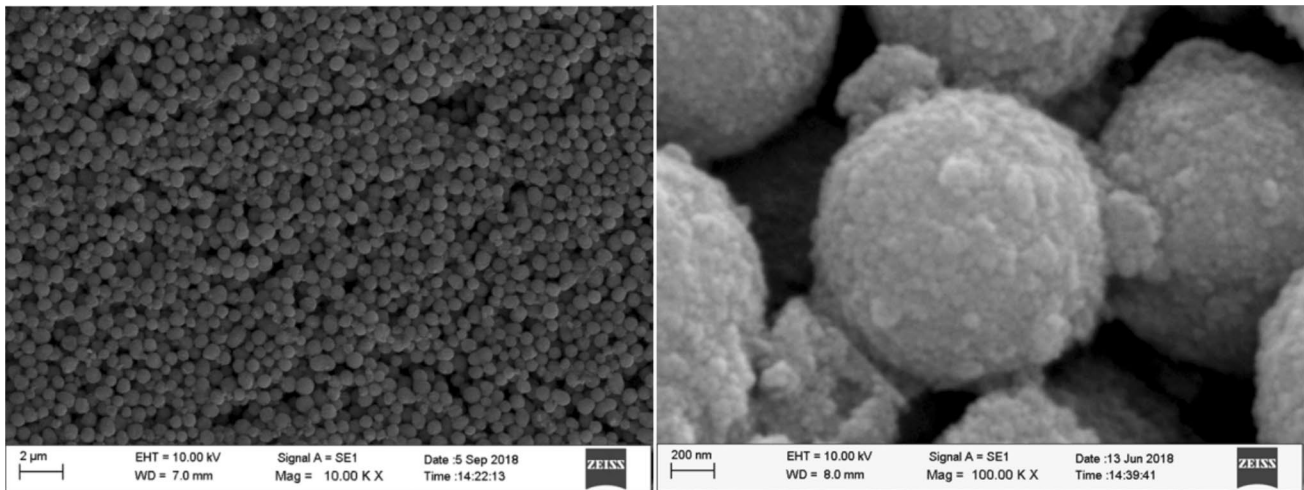


Fig. 1 **a** SEM image of as-prepared TiO_2 microspheres; **b** HRSEM image of a single TiO_2 microsphere of diameter around 700 nm consisting of small TiO_2 nanoparticles of average diameter 5–15 nm

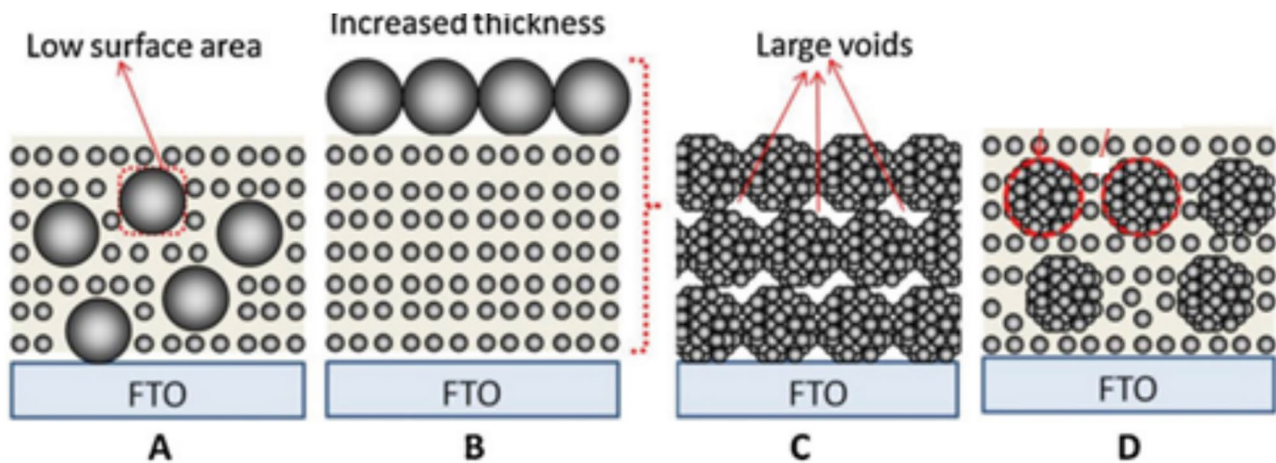


Fig. 2 Schematic diagrams of four different types of photoanodes fabricated with microsphere light scatterers mixed with nanoparticles to be used as possible photoanodes in DSSCs [33]

TiO_2 microspheres mixed with nanoparticles for better inter-grain connectivity in addition to the increased surface area and enhanced light scattering.

The light scattering in schemes A and B is achieved with the aid of the large solid microspheres. However, these solid spheres have low surface area for dye loading and also the thickness of the photoanode increases if the microspheres are arranged as the additional top layer as shown in scheme B. In a thicker photoanode, the photo-generated charge carriers have to travel a longer distance to reach electrodes, and in this process, many carriers may get lost due to recombination. On the other hand, the hierarchically structured TiO_2 microspheres consisting of aggregates of smaller nanoparticles provide both a larger effective specific surface area and a high light scattering effect. However, in the photoanode structure illustrated in schematic C, large voids exist between the microspheres seen

in the photoanode compared to a photoanode fabricated only with conventional TiO_2 P25 nanoparticles as illustrated in the bilayer structure in scheme B. The presence of such voids as shown in scheme C would result in a low inter-grain connectivity for effective charge transfer between the microspheres.

Therefore, as indicated by the above schemes, the composite structure shown in scheme D appears to minimize the drawbacks inherent in the other three possible photoanode structures. Hierarchically structured TiO_2 microspheres effectively increase the light scattering without significantly sacrificing the available surface area for dye adsorption, and the incorporation of smaller TiO_2 nanoparticles in the microspheres increases the connectivity among all the TiO_2 particles for efficient electron transport. Moreover, scheme D increases the amount of dye adsorption per unit area of the photoanode without increasing the overall photoanode film

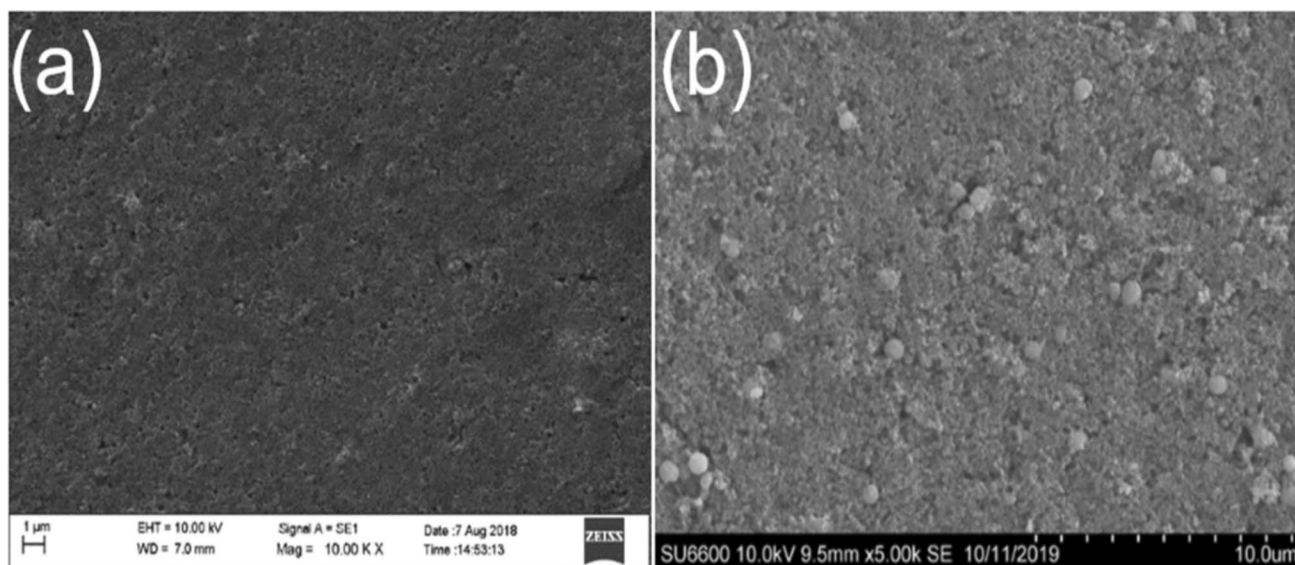


Fig. 3 SEM image of **a** P25 photoanode and **b** 10% MS + 90% P25 composite photoanode consisting of TiO₂ microspheres (MS) and TiO₂ P25 particles

thickness. Taking this unique multifunctional nature of the photoanode of scheme D of Fig. 2 into account, the composite photoanode structure D consisting of hierarchically structured TiO₂ microspheres (MS) embedded in the TiO₂ nanoparticle (P25) medium has been adopted in this work as a novel photoanode structure and used throughout this study. Figure 3 shows the SEM images of the P25 TiO₂ nanoparticle-based conventional photoanode used as the reference and the optimized composite photoanode consisting of 10 wt% of TiO₂ microspheres (MS) and 90 wt% of TiO₂ P25 nanoparticles.

It can be seen from Fig. 3b that the TiO₂ P25 nanoparticles and TiO₂ microspheres (MS) are mixed homogeneously, and there are no visible voids or cracks in the photoanode structure. However, it is quite likely that a further increase in the amount of TiO₂ microspheres in the mixture would have resulted in the agglomeration of microspheres and developed minor cracks in the photoanode. These cracks could eventually cause hindrances for electronic transport and charge transfer within the photoanode. The optimized composition with 10% MS was therefore selected for further studies.

Diffuse reflectance spectroscopy of MS/P25 photoanodes

Light scattering properties of TiO₂ microspheres in the composite photoanodes were investigated using diffuse reflectance spectroscopy. As depicted in Fig. 4, the diffuse reflectance of the photoanode has increased as the amount of TiO₂ microspheres present in the composite increases. All three composite photoanodes with different content of TiO₂ microspheres exhibit higher diffuse reflectance than the reference photoanode

fabricated with only P25 nanoparticles. The photoanode with 10 wt% of MS content shows the highest diffuse reflectance in the wavelength range between 550 and 800 nm. The increase in light scattering ability of the photoanode increases the effective optical path length within the photoanode through multiple light scattering. This provides the so-called ‘light trapping effect’ within the photoanode thereby increasing the probability of light absorption. The diffuse reflectance results are consistent with the current–voltage characteristics of the DSSCs.

Optical absorption of silver nanoparticles

Figure 5 shows the UV–visible absorption spectra of silver nanoparticles dispersed in ethanol. The orange colour AgNPs seed solution has an absorption peak at 422 nm. When the seed solution was heated at 90 °C, the reaction solution first turned to red colour (540 nm) in 2 h and then to blue colour (598 nm) in 4 h. The absorption peak of the seed solution of AgNPs has red-shifted and broadened with increasing the reaction time. This indicates that the shape and size of the nanoparticles increases with reaction time as observed and reported by others [34, 36].

This is primarily due to the phenomenon known as localized surface plasmon resonance (LSPR). When silver nanoparticles are exposed to light, the conduction electrons on the surface oscillate collectively in resonance with the incident light’s electromagnetic field. This collective oscillation is called LSPR. The LSPR frequency depends on the size, shape, and dielectric environment of the nanoparticles. These observed peak positions match very well with peak values for each colour as reported in the literature [34, 36].

Fig. 4 Diffuse reflectance spectra of TiO₂ P25/MS composite photoanodes with different percentages of TiO₂ MS. **a** P25 only, **b** 5 wt% MS + 95 wt% P25, **c** 10 wt% MS + 90 wt% P25, and **d** 15 wt% MS + 85 wt% P 25

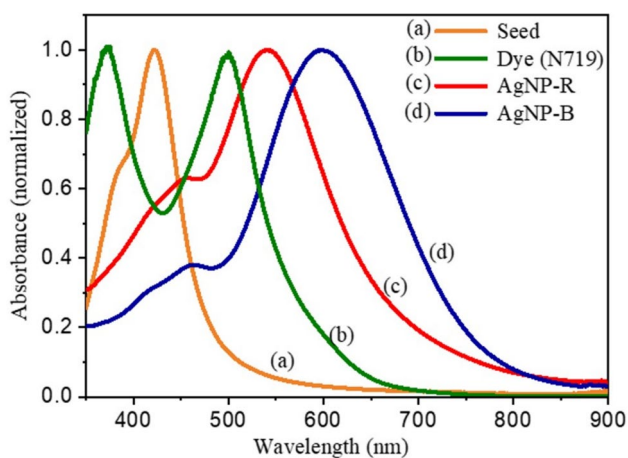
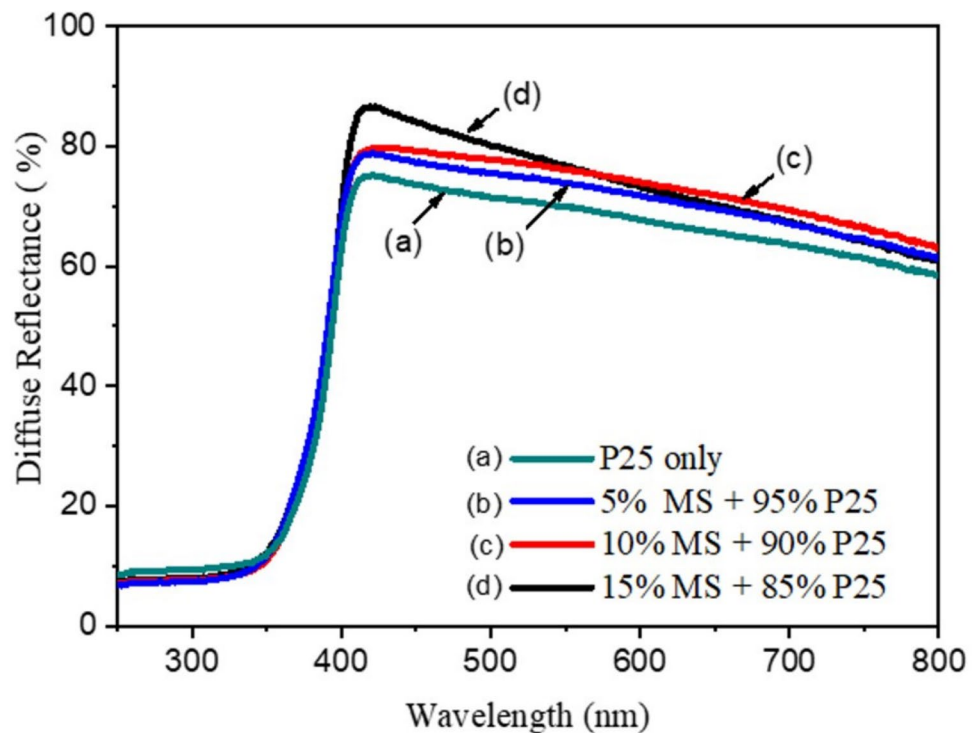


Fig. 5 UV-visible optical absorption spectra of silver nanoparticles dispersed in ethanol, **a** seed (c) red colour, **d** blue colour, and **b** N719 dye dissolved in ethanol

It should be noted that the plasmonic absorption peaks of both red and blue AgNPs are located in the region where the absorption of N719 dye is very weak.

Optical absorption of AgNPs incorporated photoanodes

UV-VIS absorption spectra of (a) bare TiO₂ photoanode, (b) AgNP loaded TiO₂ photoanode, (c) dye adsorbed TiO₂ photoanode, and (d) AgNP loaded dye adsorbed TiO₂

photoanode are shown in Fig. 6. The absorption spectrum of the blue AgNP (80 nm) loaded TiO₂ indicates that the incorporation of the plasmonic AgNP induces a higher and the broader absorption compared to that of the reference bare TiO₂ photoanode. The observed data undisputedly reveal that the enhancement of light absorption is due to the presence of plasmonic AgNPs in the photoanode. The absorption of the peak of N719 dye is slightly blue-shifted upon the incorporation of AgNPs which could be due to the surface modification by the incorporation of AgNPs [36]. A similar effect was observed with red-coloured silver nanoparticles (AgNP, size, 20 nm). As the performance of the DSSCs made from TiO₂ incorporated with blue-coloured AgNPs was better, some of the photoanode characterizations were limited to the TiO₂ incorporated with blue-coloured AgNPs only.

From the Tauc plot method based on the assumption that the energy-dependent absorption coefficient α can be expressed by the equation $(\alpha \cdot h\nu)^{0.5} = B(h\nu - E_g)$, the band gap energies of pristine TiO₂ (an indirect band gap semiconductor) and the TiO₂ incorporated with plasmonic Ag NPs can be estimated. Figure 7 shows the Tauc plot based on the diffuse reflection data for these two photoanodes. Based on the points of intersection of the linear part of the graphs on the x-axis, the estimated energy band gap values are 2.90 eV for the pristine TiO₂ and 2.75 eV for the Ag NP incorporated TiO₂ [37]. This shows that in addition to the enhanced optical absorption mediated by the plasmonic effect, AgNPs have also contributed to the increased visible light absorption due to the energy band gap narrowing. Ag-doped TiO₂ thin films have shown enhanced photocatalytic

Fig. 6 UV–Visible absorbance spectra of (a) TiO₂ photoanode, (b) TiO₂ photoanode incorporated with blue AgNPs, (c) dye adsorbed TiO₂ photoanode, and (d) dye adsorbed blue AgNPs incorporated TiO₂ photoanode

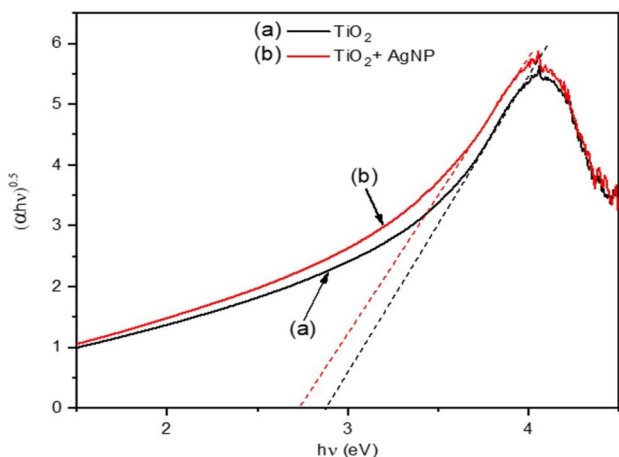
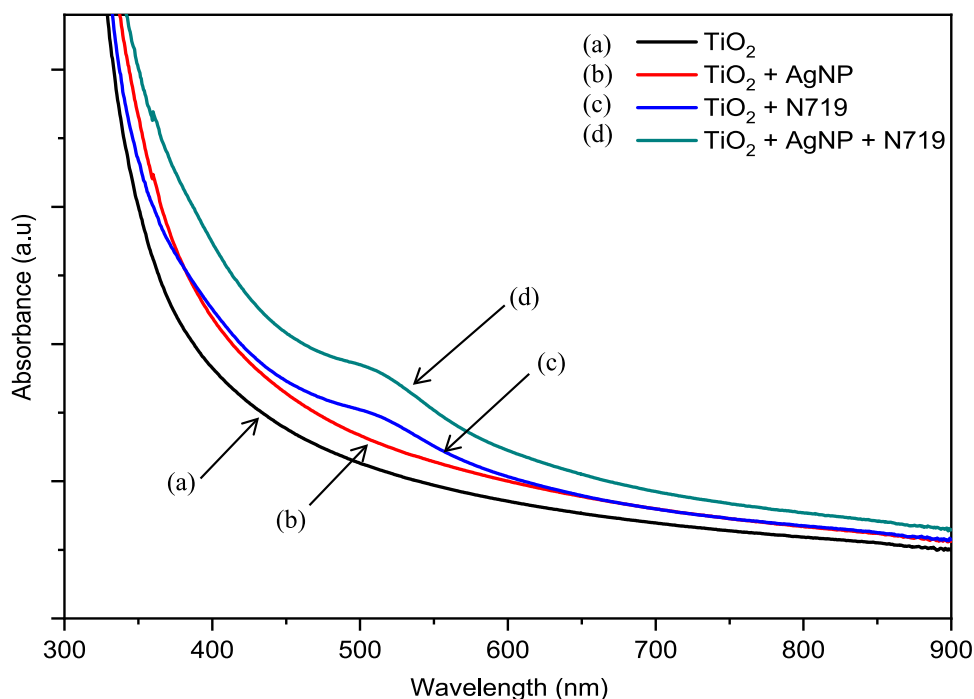


Fig. 7 The Tauc plot of $(\alpha \cdot hv)^{0.5}$ vs photon energy (hv) from the UV–Visible diffuse reflection data for (a) pristine TiO₂ photoanode and (b) TiO₂ photoanode incorporated with blue AgNPs

behaviour due to their medium band gap energy (3.17–2.75 eV) and also providing high surface area (85–231 m²/g) [38].

TEM analysis of colloidal AgNPs

The shapes and sizes of the synthesized AgNPs were analyzed using TEM imaging. Figure 8 shows the TEM images of as-synthesized AgNPs in ethanol. The average particle sizes of the red-coloured AgNPs and the blue-coloured clustered AgNPs were about 20 nm and 80 nm, respectively.

The shape (sphere) and the size of the red colour AgNPs are consistent with the data reported in the literature, namely, ~20 nm [33–35]. However, the blue colour AgNPs in our work appear to be nanoparticle aggregates with a diameter of around ~80 nm.

XRD analysis of AgNPs incorporated MS/P25 photoanode

Figure 9 shows the X-ray diffraction patterns of P25 and P25/MS/Ag thin films. The diffraction peaks present at 25.3°, 37.8°, 48°, 53.9°, 55.1°, 62.7°, and 68.6° were observed and indexed by matching with reference database (JCPDS No.21–1272) which confirms the presence of anatase and rutile phases of TiO₂. It is also found that the Ag characteristic peaks are not visible in the XRD spectrum of MS/P25/Ag film, quite likely due to the very small amount of Ag present in the TiO₂ thin film (0.10% (W/V) in the precursor solution). Also, the prominent XRD peaks of silver generally occurs at 38.1° (111), 44.3° (200), and 64.4° (220) [37, 38]. Even if these peaks are present, they can overlap with and be masked by TiO₂ peaks.

EDX analysis of AgNPs incorporated MS/P25 photoanode

Figure 10 shows the EDX spectrum of AgNP incorporated MS/P25 composite TiO₂ photoanode. It confirms the presence of Ag in the photoanode.

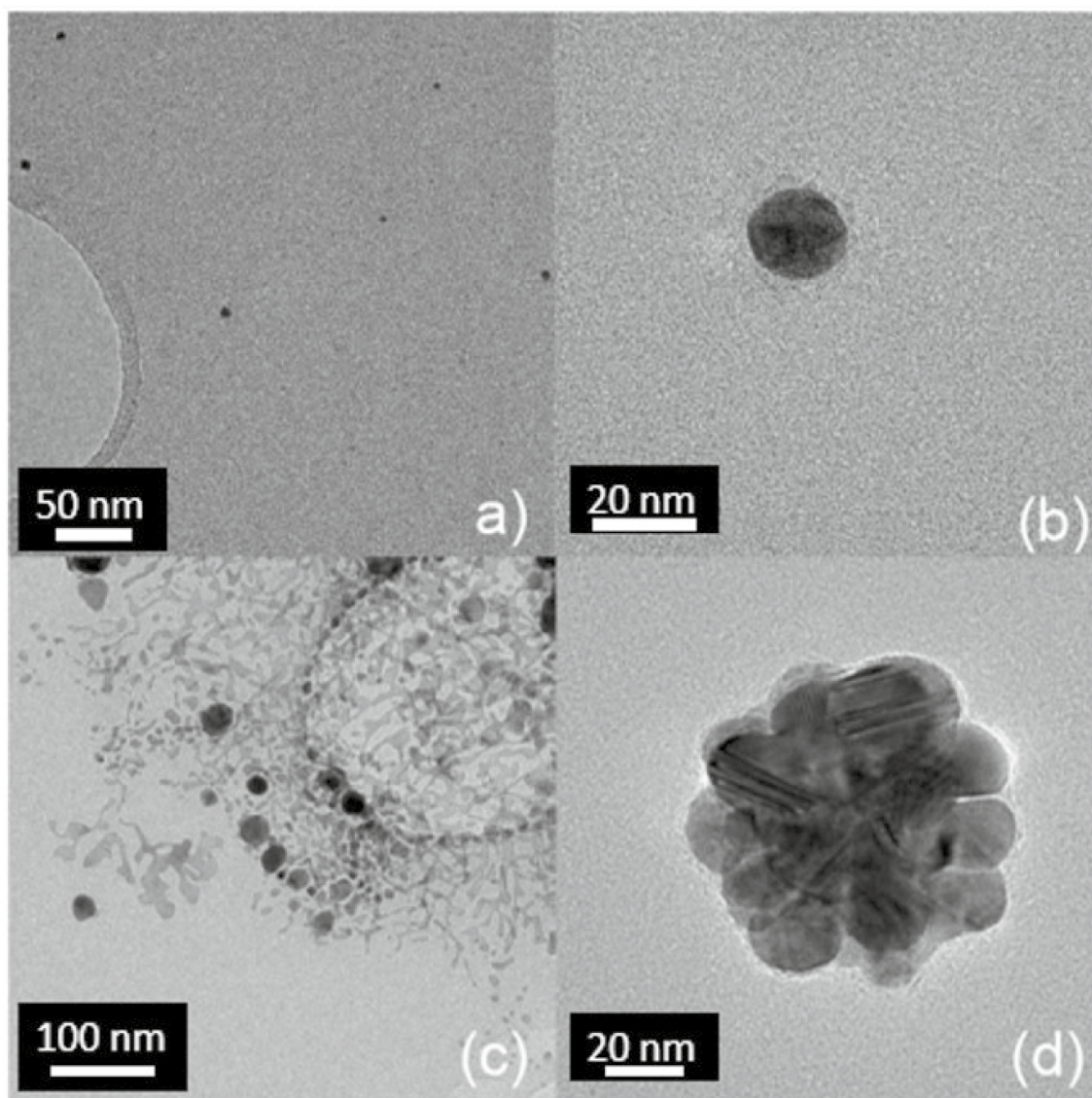


Fig. 8 TEM images of AgNPs dispersed in ethanol: **a, b** AgNP—red; **c, d** AgNP—blue

Furthermore, EDX elemental mapping was taken to see the spatial distribution of AgNPs on the photoanode, and Fig. 11d reveals that AgNPs are uniformly distributed within the photoanode.

I-V characterization

Figure 11 shows the current density–voltage (I - V) characteristics of DSSCs fabricated with composite photoanodes having different amounts of TiO_2 microspheres measured under 100 mW cm^{-2} light illuminations. The detailed solar cell parameters extracted from the figure are summarized in Tables 1 and 2. DSSC fabricated with 10% MS TiO_2 added photoanode exhibited the highest current density of 15.01 mA cm^{-2} with an efficiency of 7.17%. This could

be attributed to the enhanced light absorption due to superior light scattering ability of microspheres which is also confirmed by the diffuse reflectance measurements. The slight decrease in the open circuit voltage and fill factor of composite cells could be due to the increased recombination of charge carriers due to microspheres.

Dwivedi et al. have reported that TiO_2 hollow spheres, synthesized using a continuous spray pyrolysis reactor, were successfully utilized as a scattering layer in dye-sensitized solar cells (DSSC) to enhance their photovoltaic performance. The use of the TiO_2 hollow spheres of diameter about 170–300 nm has shown improved power conversion efficiency of 7.46% which is higher than cells made with conventional TiO_2 P25 photoanode (7.1%). This has been attributed to TiO_2 hollow spheres acting as a

Fig. 9 XRD patterns of P25 and P25/MS/Ag thin films

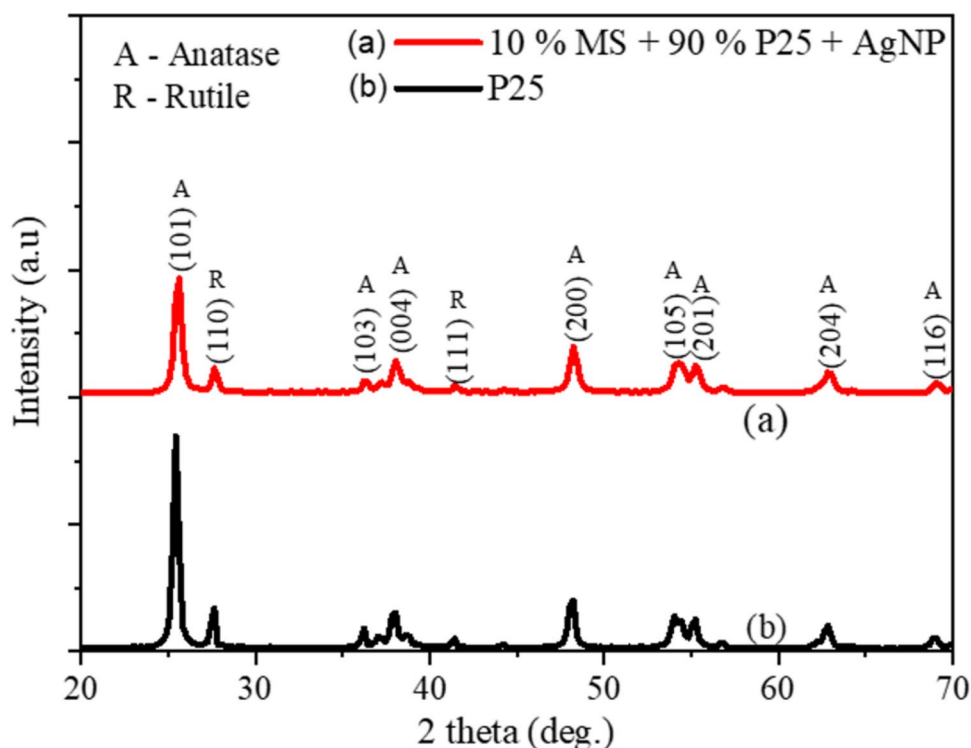
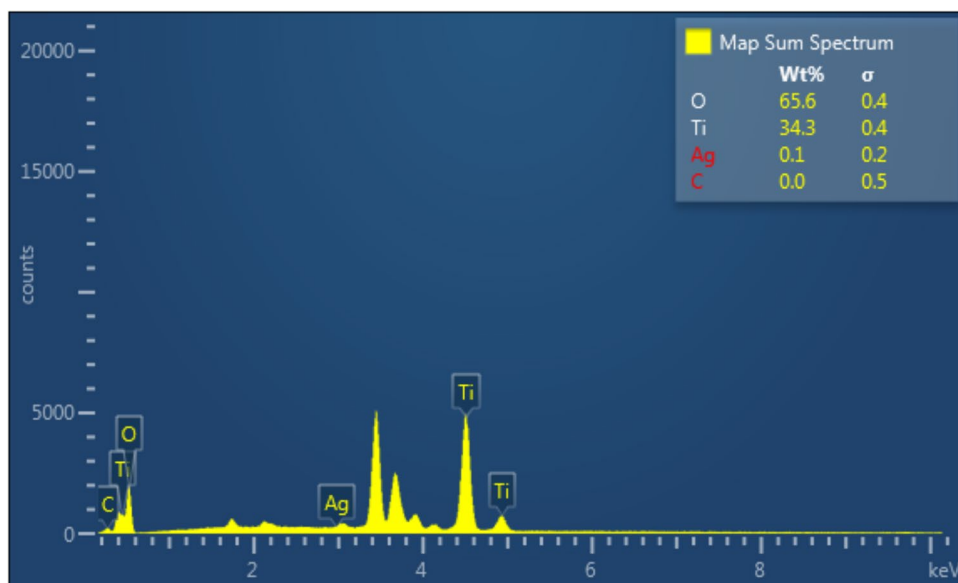


Fig. 10 EDX spectra of AgNP incorporated MS/P25 composite photoanode



light-scattering layer to enhance the light-harvesting and photovoltaic performance of the DSSCs [26].

To see the effect of the incorporation of plasmonic-induced light absorption on the performances of the DSSCs, current density–voltage characteristics (J - V) of the DSSCs fabricated with AgNPs were measured, and results are illustrated in Fig. 12. As shown in Fig. 13, a significant increase in the short-circuit photocurrent density (J_{sc}) can be seen in the DSSCs fabricated with plasmonic silver nanoparticle-incorporated photoanodes compared to the DSSCs made

with photoanodes without AgNPs. These results are summarized in Table 1. The DSSCs incorporated with blue AgNPs (~ 80 nm) showed an enhancement in the efficiency from 7.17 to 8.15%, which accounts for the highest enhancement in the efficiency by $\sim 14\%$ whereas the red coloured AgNPs incorporation showed an efficiency enhancement from 7.17 to 7.88%. However, by considering the combined effect of the incorporation of MS the AgNPs (Blue) and AgNPs (red) showed an impressive $\sim 29\%$ and $\sim 24\%$ overall efficiency enhancement, respectively as shown in bold letter in Table 2.

Fig. 11 EDX elemental mapping of AgNP incorporated MS/P25 composite photoanode showing the presence of elements **a** C, **b** Ti, **c** O, and **d** Ag

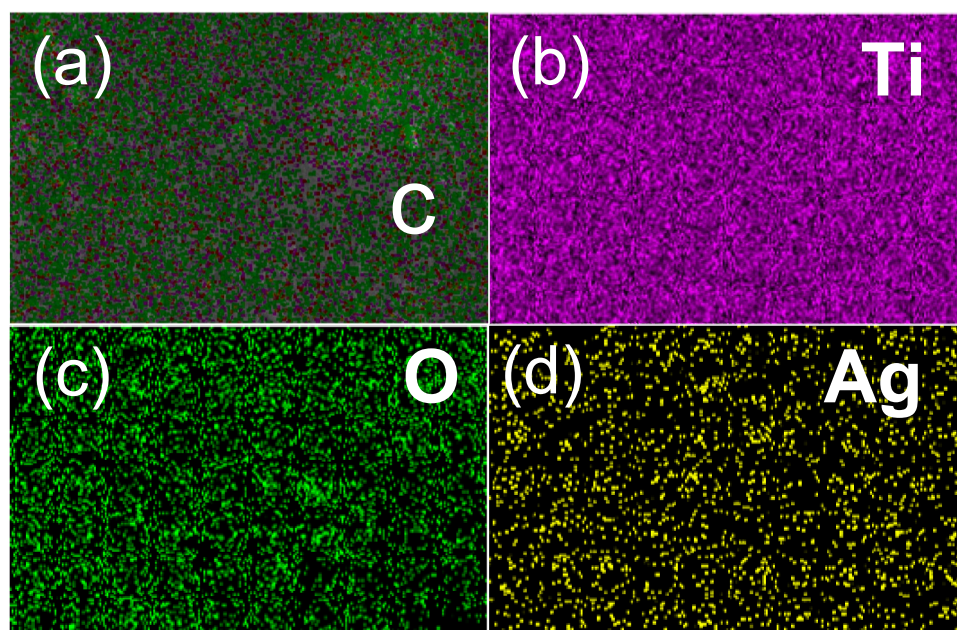


Table 1 Photovoltaic parameters of double layer and single layer DSSCs

| Photoanode | J_{SC} (mA cm ⁻²) | V_{OC} (mV) | FF (%) | Efficiency (%) |
|-------------------------|---------------------------------|---------------|----------|----------------|
| P25 only | 12.52 | 736.6 | 68.70 | 6.34 |
| 5 wt% MS | 14.48 | 728.1 | 66.01 | 6.96 |
| 10 wt% MS | 15.01 | 732.1 | 65.30 | 7.17 |
| 15 wt% MS | 13.78 | 730.3 | 65.56 | 6.60 |
| 10 wt% MS + AgNP (red) | 16.43 | 722.4 | 66.42 | 7.88 |
| 10 wt% MS + AgNP (blue) | 17.93 | 736.7 | 61.90 | 8.15 |

Table 2 EIS parameters of composite photoanode based DSSCs with and without Ag plasmonic nanoparticles

| TiO ₂ photoanode | R_S (Ω) | R_1 (Ω) | R_2 (Ω) | f_{max} (Hz) | τ (ms) | Eff (%) |
|-----------------------------|--------------------|--------------------|--------------------|----------------|-------------|-------------|
| P25 | 18.1 | 7.6 | 24.8 | 18.47 | 8.62 | 6.34 |
| 10 wt% MS | 13.6 | 8.2 | 21.7 | 18.41 | 8.64 | 7.17 |
| 10 wt% MS + AgNP (red) | 11.0 | 7.9 | 15.5 | 22.40 | 7.11 | 7.88 |
| 10 wt% MS + AgNP (blue) | 10.5 | 11.5 | 17.6 | 26.88 | 5.92 | 8.15 |

The increase in the J_{sc} observed in the DSSCs fabricated with these photoanodes should essentially be due to the enhancement of light absorption by the local surface plasmon resonance (LSPR) effect by the Ag nanoparticles in the photoanode with some contributions from the energy band gap narrowing caused by the presence of AgNPs as discussed above. The LSPR effect improves the light absorption cross-section of the dye molecules by enhancing the light intensity in the near field, which subsequently increases the photon absorption,

which in turn improves the photoelectron generation in the TiO₂ photoanode.

Electrochemical impedance spectroscopic (EIS) analysis

The electrochemical impedance spectroscopic (EIS) studies were performed on DSSCs fabricated with and without the Ag NPs in the composite 10% MS/P25 photoanodes under

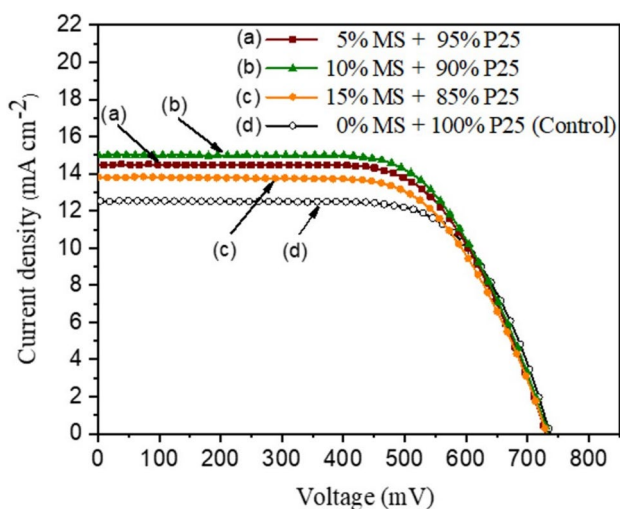


Fig. 12 Current density–voltage (J - V) characteristics of the DSSCs fabricated with photoanodes containing different percentages of MS content

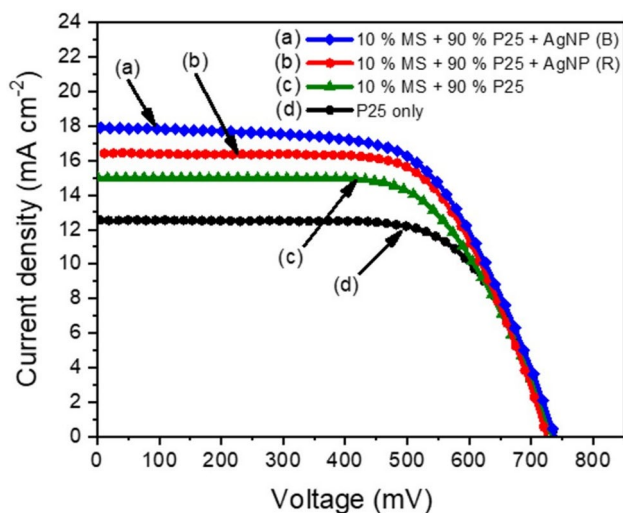


Fig. 13 Current density–voltage (J - V) characteristics of the DSSCs fabricated with photoanodes containing AgNP incorporated and MS/P25 optimized TiO₂ photoanode

100 mW cm⁻² light illumination with AM 1.5 filter at open circuit condition. Figure 14a, b shows the Nyquist plots and Bode phase plots extracted from EIS spectra. The first semicircle in Fig. 14a corresponds to the charge transfer resistance (R_1) at the electrolyte/Pt counter electrode interface, and the second semicircle is attributed to charge transfer resistance (R_2) at the dye-TiO₂/ electrolyte interface. It can be noted that there are no significant changes in the characteristic of the first semicircle (R_1) other than the different intersection points at the real part of the impedance (Z) axis. This observation can be justified as we have used the

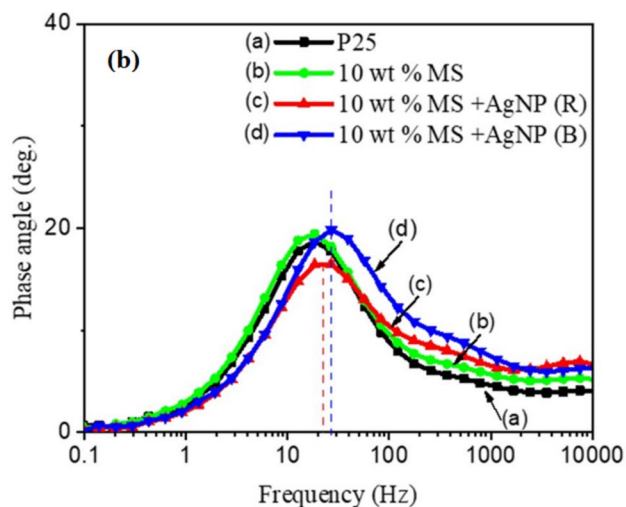
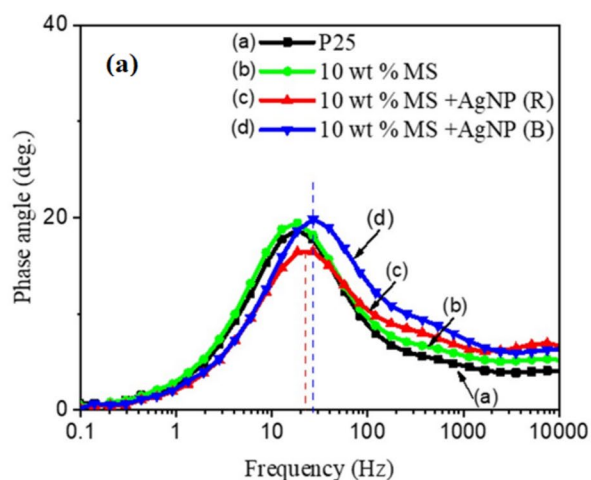


Fig. 14 **a** Nyquist plot and **b** Bode plots of DSSCs fabricated with TiO₂ photoanodes with optimum composition of MS/P25, with and without AgNPs measured under 100 mW cm⁻² illumination

same electrolyte and the same Pt counter electrodes in all the DSSCs. There is a significant reduction in the diameter of the second semicircle associated with charge transfer resistance (R_2) at the dye-TiO₂/ electrolyte interface indicating lower charge transfer resistance for the AgNPs-based DSSCs. These data further confirm that the presence of Ag nanoparticles in the TiO₂ thin film improves the charge separation process in the photoanode and thereby enhances the electron transport process and contributes to the overall efficiency enhancement in the AgNPs-based DSSCs. The charge transfer resistance R_2 (17.6 Ω) of blue colour AgNP incorporated DSSC is slightly higher than that of the red colour AgNP incorporated DSSC (15.5 Ω). This increase may be due to the aggregation of blue colour AgNPs as shown in Fig. 7 (d).

The electron lifetimes of above DSSCs estimated from Bode phase plots are given in Table 2. It can be observed

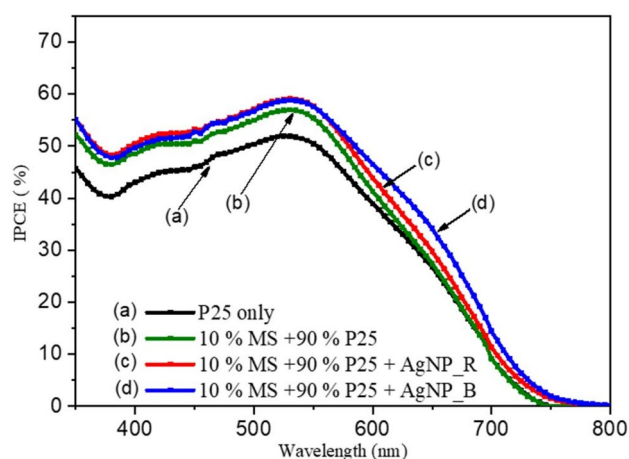


Fig. 15 IPCE curves for DSSCs made with photoanodes of optimum composition MS/P25 DSSC with and without AgNPs

that upon the addition of the Ag/NPs in the photoanode, the electron life time has reduced. This could be due to high charge recombination at metal–semiconductor interface. However, despite the lower electron lifetime in the DSSCs with AgNP incorporated photoanode, the overall efficiency has increased as a result of the efficient and improved electron transfer due to the incorporation of AgNPs.

Incident photon to electron conversion efficiency (IPCE) analysis

To study the effect of incorporation of AgNPs on the incident photon to electron conversion efficiency (IPCE) of the DSSCs, IPCE spectra of DSSCs fabricated with four different photoanodes, (a) P25 TiO₂ nanoparticles, (b) 10% MS TiO₂ particles + 90% P25 TiO₂ nanoparticles composite, (c) 10% MS TiO₂ particles + 90% P25 TiO₂ nanoparticles composite with red colour silver nanoparticles, and (d) 10% MS TiO₂ particles + 90% P25 TiO₂ nanoparticles composite with blue colour silver nanoparticles were obtained. As shown in Fig. 15, all four devices show the maximum IPCE value around the wavelength 530 nm, which is attributed to the characteristic peak of the N719 dye. The IPCE spectra of DSSC made with 10% MS TiO₂ particles + 90% P25 TiO₂ nanoparticle composite show higher IPCE values than the DSSC made with only P25 TiO₂ nanoparticles over almost the entire wavelength region. This is consistent with a higher current density value exhibited by the former as observed in the *J*-*V* curves shown in Fig. 12. This enhancement in IPCE can be attributed to better utilization of light in composite photoanode upon inclusion of MS particles at optimum ratio. The composite photoanode produces a maximum IPCE of 57% at a wavelength of 530 nm while the DSSC made

of only P25 TiO₂ nanoparticles exhibits an IPCE of 52%. As expected, the IPCE spectrum of DSSCs made of silver nanoparticles incorporated in composite photoanodes shows higher values compared to the composite photoanode made without silver nanoparticles. The IPCE spectrum of red-coloured silver nanoparticle incorporated DSSC only shifted along the vertical axis by some factor concerning composite photoanode without silver nanoparticles. This could be due to the absorption peak of N719 dye and red-coloured silver nanoparticles appearing at nearly the same wavelengths. However, there was a considerable enhancement in IPCE observed with the incorporation of blue-coloured silver nanoparticles in the long wavelength range from 550 to 800 nm consistent with the UV visible absorption spectrum as shown in Fig. 5.

Conclusion

Performance of the DSSCs fabricated with composite photoanodes consisting of P25 TiO₂ nanoparticles and hierarchical TiO₂ microspheres (MS) at different concentrations 0, 5, 10, and 15 wt% was investigated. The average diameter of the microspheres was found to be about 700 nm consisting of aggregates of smaller TiO₂ nanoparticles of diameters in the 5–15 nm range. It was found that photoanodes fabricated by incorporating 10 wt% TiO₂ mesospheres to the conventional P25 photoanode enhanced device efficiency by 13%. When silver nanoparticles with two different sizes with red and blue colour were incorporated into the optimized composite photoanode made with P25 and 10 wt% TiO₂ mesospheres, impressive efficiency enhancements of 24% and 29% respectively were obtained for the red colour AgNPs and the blue colour AgNPs. This significant efficiency increase has been attributed to the improved light absorption due to the scattering effect by large diameter TiO₂ (MS) mesospheres, increase in specific surface area due to constituent microstructure with small diameter TiO₂ nanoparticle aggregates together with the plasmonic effect by silver nanoparticles.

Funding This research is supported by a postgraduate research scholarship award (NSF/SCH/2019/5) by the National Science Foundation, Sri Lanka.

Data availability Original data related to this work is available on request from the corresponding author.

Declarations

Competing interest The authors declare that they have no known competing financial interests or personal relationships that could have appeared to influence the work reported in this paper.

References

- O'Regan B, Grätzel M (1991) A low-cost, high-efficiency solar cell based on dye-sensitized colloidal TiO₂ films. *Nature* 353(6346):737–740
- Grätzel M (2001) Photoelectrochemical cells. *Nature* 414:338–344
- Hagfeldt A, Boschloo G, Sun L, Kloo L, Pettersson H (2010) Dye-sensitized solar cells. *Chem Rev* 110(11):6595–6663
- Yella A, Lee HW, Tsao HN, Yi C, Chandiran AK, Nazeeruddin MK (2011) Porphyrin-sensitized solar cells with cobalt (II/III)-based redox electrolyte exceed 12 percent efficiency. *Science* 334(6056):629–634
- Mathew S, Yella A, Gao P, Humphry-Baker R, Curchod BFE, Ashari-Astani N et al (2014) Dye-sensitized solar cells with 13% efficiency achieved through the molecular engineering of porphyrin sensitizers. *Nat Chem* 6:242–247
- Kakiage K, Aoyama Y, Yano T, Oya K, Fujisawa J, Hanaya M (2015) Highly-efficient dye-sensitized solar cells with collaborative sensitization by silyl-anchor and carboxy-anchor dyes. *Chem Comm* 51(88):15894–15897
- Dwivedi C, Dutta V, Chandiran AK et al (2013) Anatase TiO₂ hollow microspheres fabricated by continuous spray pyrolysis as a scattering layer in dye-sensitized solar cells. *Energy Procedia* 33:223–227
- Liu ZH, Su XJ, Hou GL, Bi S, Xiao Z, Jia HP (2012) Enhanced performance for dye-sensitized solar cells based on spherical TiO₂ nanorod-aggregate light-scattering layer. *J Power Sources* 218:280–285
- Jiang J, Gu F, Ren X, Wang Y, Shao W, Li C et al (2011) Efficient Light Scattering from One-Pot Solvothermally Derived TiO₂ Nanospindles. *Ind Eng Chem Res* 50:9003–9008
- Yum JH, Baranoff E, Kessler F et al (2012) A cobalt complex redox shuttle for dye-sensitized solar cells with high open-circuit potentials. *Nat Commun* 3:631
- Dissanayake MAKL, Thotawatthage CA, Senadeera GKR, Bandara TMWJ, Jayasundera WJMJSR, Mellander B-E (2012) Efficiency enhancement by mixed cation effect in dye-sensitized solar cells with PAN based gel polymer electrolyte. *J Photochem Photobiol A* 246:29–35
- Wang H, Sun K, Tao F, Stacchiola DJ, Hu YH (2013) 3D honeycomb-like structured graphene and its high efficiency as a counter-electrode catalyst for dye-sensitized solar cells†. *Angew Chem Int Ed* 52:9210–9214
- Murakami TN, Ito S, Wang Q, Nazeeruddin MK, Bessho T, Cesar I (2006) Highly efficient dye-sensitized solar cells based on carbon black counter electrodes. *J Electrochem Soc* 153:A2255–A2261
- Grätzel M (2009) Recent advances in sensitized mesoscopic solar cells. *Acc Chem Res* 42(11):1788–1798
- Usami A (2000) A theoretical simulation of light scattering of nanocrystalline films in photoelectrochemical solar cells. *Sol Energy Mater Sol Cells* 62:239–246
- Ito S, Murakami TN, Comte P, Liska P, Grätzel M, Nazeeruddin MK (2008) Fabrication of thin film dye sensitized solar cells with solar to electric power conversion efficiency over 10%. *Thin Solid Films* 516:4613–4619
- Qiu Y, Chen W, Yang S (2010) Double-layered photoanodes from variable-size anatase TiO₂ nanospindles: a candidate for high-efficiency dye-sensitized solar cells. *Angew Chem Int Ed* 49:3675–3679
- Yang L, Lin Y, Jia JG, Xiao XR, Li XP, Zhou XW (2008) Light harvesting enhancement for dye-sensitized solar cells by novel anode containing cauliflower-like TiO₂ spheres. *J Power Sources* 182:370–376
- Zhang Z, Ito S, O'Regan B, Kuang D, Zakeeruddin SM, Liska P, Charvet R, Comte P, Nazeeruddin MK, Péchy P, Humphry-Baker R, Koyanagi T, Mizuno T, Grätzel M (2007) The electronic role of the TiO₂ light-scattering layer in dye-sensitized solar cells. *J Phys Chem* 221(3):319–327
- Bakhshayesh AM, Mohammadi MR, Dadar H, Fray DJ (2013) Improved efficiency of dye-sensitized solar cells aided by corn-like TiO₂ nanowires as the light scattering layer. *Electrochim Acta* 90:302–308
- Zhang W, Xie Y, Xiong D, Zeng X, Li Z, Wang M, Cheng YB, Chen W, Yan K, Yang S (2014) TiO₂ nanorods: a facile size- and shape-tunable synthesis and effective improvement of charge collection kinetics for dye-sensitized solar cells. *ACS Appl Mater Interfaces* 6:9698–9704
- Sun KC, Qadir MB, Jeong SH (2014) Hydrothermal synthesis of TiO₂ nanotubes and their application as an over-layer for dye-sensitized solar cells. *RSC Adv* 4:23223–23230
- Zhu P, Nair AS, Yang S, Peng S, Ramakrishna S (2011) Which is a superior material for scattering layer in dye-sensitized solar cells, electrospun rice grain- or nanofiber-shaped TiO₂? *J Mater Chem* 21:12210
- Peng J-D, Shih P-C, Lin H-H, Chuan-Ming Tseng R, Vittal VS, Ho K-C (2014) TiO₂ nanosheets with highly exposed (001)-facets for enhanced photovoltaic performance of dye-sensitized solar cells. *Nano Energy* 10:212–221
- Al-Attafi K, Nattestad A, Yamauchi Y, Dou SX, Kim JH (2017) Aggregated mesoporous nanoparticles for high surface area light scattering layer TiO₂ photoanodes in dye-sensitized solar cells. *Sci Rep* 7:10341
- Ding Y, Mo L, Tao L, Ma Y, Hu L, Jiang L (2014) TiO₂ sub-microspheres as a bi-functional scattering layer for high performance dye-sensitized solar cells. *NANO* 9(5):1440007
- Dissanayake MAKL, Senthuran S, Senadeera GKR (2020) Efficiency enhancement in dye-sensitized solar cells using hierarchical TiO₂ submicron size spheres as a light scattering layer. *J Solid State Electrochem* 24:2261–2269
- Tan B, Wu Y (2006) Dye-sensitized solar cells based on anatase TiO₂ nanoparticle/nanowire composites. *J Phys Chem B* 110:15932–15938
- Jarka P, Drygała A, Szindler M, Tański T, Matysiak W (2020) Influence of screen printed nanowires/nanoparticles TiO₂ nanocomposite layer on properties of dye-sensitized solar cells. *Acta Phys Pol A* 138:312–316
- Yen YC, Ko WY, Chen JZ, Lin KJ (2013) Enhancing the performance of dye-sensitized solar cells based on TiO₂ nanotube/nanoparticle composite photoanodes. *Electrochim Acta* 105:142–148
- Joshi P, Zhang L, Davoux D, Zhu Z, Galipeau D, Fong H, Qiao Q (2010) Composite of TiO₂ nanofibers and nanoparticles for dye-sensitized solar cells with significantly improved efficiency. *Energy Environ Sci* 3:1507–1510
- Liu Z, Su X, Hou G, Bi S, Xiao Z, Jia H (2013) Mixed photoelectrode based on spherical TiO₂ nanorod aggregates for dye-sensitized solar cells with high short-circuit photocurrent density. *RSC Adv* 3:8474–8479
- Xi J, Zhang Q, Park K, Sun Y, Cao G (2011) Enhanced power conversion efficiency in dye-sensitized solar cells with TiO₂ aggregates/nanocrystallites mixed photoelectrodes. *Electrochim Acta* 56:1960–1966
- Joshi DN, Ilaiyaraja P, Sudakar C, Prasath RA (2018) Facile one-pot synthesis of multi-shaped silver nanoparticles with tunable ultra-broadband absorption for efficient light harvesting in dye-sensitized solar cells. *Sol Energy Mater Sol Cells* 185:104–110
- Kumari MGCM, Perera CS, Dassanayake BS, Dissanayake MAKL, Senadeera GKR (2019) Highly efficient plasmonic dye-sensitized solar cells with silver nanowires and TiO₂ nanofibers incorporated multi-layered photoanode. *Electrochim Acta* 298:330–338

36. Huang T, Xu X-HN (2010) Synthesis and characterization of tunable rainbow colored colloidal silver nanoparticles using single-nanoparticle plasmonic microscopy and spectroscopy. *J Mater Chem* 20:9867–9876
37. Tanvi T, Aman Mahajan RK, Bedi SK, Saxena V, Ajay Singh DK, Aswal (2016) Broadband enhancement in absorption cross-section of N719 dye using different anisotropic shaped single crystalline silver nanoparticles. *RSC Adv* 6(53):48064–48071
38. Komaraiah D, Radha E, Sivakumar J, Ramana Reddy MV, Sayanna R (2020) Photoluminescence and photocatalytic activity of spin coated Ag⁺ doped anatase TiO₂ thin films. *Opt Mater* 108:110401

Publisher's Note Springer Nature remains neutral with regard to jurisdictional claims in published maps and institutional affiliations.

Springer Nature or its licensor (e.g. a society or other partner) holds exclusive rights to this article under a publishing agreement with the author(s) or other rightsholder(s); author self-archiving of the accepted manuscript version of this article is solely governed by the terms of such publishing agreement and applicable law.

Authors and Affiliations

M. A. K. L. Dissanayake¹ · S. Senthuran^{1,2,3} · G. K. R. Senadeera^{1,4}

✉ G. K. R. Senadeera
gksen@ou.ac.lk

¹ National Institute of Fundamental Studies, Kandy 20000, Sri Lanka

² Department of Physics, University of Jaffna, Jaffna 40000, Sri Lanka

³ Postgraduate Institute of Science, University of Peradeniya, Peradeniya 20400, Sri Lanka

⁴ Department of Physics, The Open University of Sri Lanka, Nawala, Nugegoda 10250, Sri Lanka